JOURNAL OF AIRCRAFT
Vol. 32, No. 6, November–December 1995

Rear Fuselage Flow Studies on a Modern Transonic Transport Aircraft

E. Coustols,* S. Prudhomme,† and A. Mignosi‡
CERT/ONERA, Toulouse 31055, France
and
D. Destarac§
ONERA, Châtillon 92322, France

An experimental program was set up in the CERT/ONERA's T2 wind tunnel, which is transonic, pressurized, and has self-adaptive walls. A 1/80th-scale model of a modern transonic transport aircraft was tested in two configurations: 1) fuselage without horizontal stabilizer and 2) fuselage with horizontal stabilizer. Various measurements were performed: oil-flow visualizations, pressure distributions, boundary-layer surveys along the fuselage symmetry lines using a three-dimensional laser Doppler anemometry system, and wake surveys with both pressure and velocity measurements in a plane downstream of the fuselage base. Moreover, both inviscid and viscous computations were carried out separately under experimental conditions. This article reports a detailed analysis of the computations and experiments conducted on the model in both configurations; the objective of this study was to reach a better understanding of the flows developing along the rear part of a fuselage.

I. Introduction

DESIGNERS have given considerable attention to three-dimensional flow separation on various parts of aircraft. Although rear-fuselage separation is less important on a commercial transport aircraft than on one with military-style, rear-loading cargo doors, it is still worth investigating because it may be a significant source of drag. It should be emphasized that three-dimensional flow separation cannot be accurately detected by observing tuft stuff during flight tests or woollen threads in a wind tunnel. Generally speaking, because three-dimensional flow separation is associated with the storage of fluid in the wall region, it causes an important vortex motion that develops near the lower symmetry line of the fuselage and, consequently, spreads downstream of the upswept fuselage base.

The experiments reported here were conducted in the test section of CERT's T2 wind tunnel, which is transonic, pressurized, and has self-adaptive walls. Tests were performed at a stagnation pressure close to 2 bar, at ambient temperature and at a freestream Mach number of 0.82. The Reynolds number, based on the aerodynamical chord length of the model, was close to 2.5×10^6. That figure is comparable to Reynolds numbers reached for industrial wind-tunnel applications, but of course is less than the flight Reynolds number, which is close to 5×10^7.

For each model configuration ("fuselage without stabilizer" and "fuselage with stabilizer"), a number of measurements were performed: oil-flow visualizations, pressure distributions, boundary-layer surveys along the upper and lower symmetry lines using the three-dimensional laser Doppler anemometry (LDA) system, and wake surveys with both pressure and velocity measurements in a plane located at approximately two diameters downstream of the fuselage base.

Moreover, both inviscid and viscous computations were carried out under experimental conditions, but no coupling method has yet been developed. The external flow was computed using a surface panel method, while the local three-dimensional boundary-layer equations were solved using a characteristic method.

This article presents detailed results of both the experiments and the computations conducted for each model configuration tested. That work had two main goals: first, to reach a better understanding of the external and wall flows developing along the rear fuselage of a commercial-type subsonic aircraft; and second, to generate an important database necessary for validating present and future inviscid and viscous codes used and developed at ONERA.

It should be pointed out that these experiments are the first (to our knowledge) dealing with the effect of the horizontal stabilizer on the wall flow in the rear part of the fuselage.

II. Wind-Tunnel Conditions

A. Experimental Setup Model

1. T2 Wind Tunnel

The T2 wind tunnel (at the Aerothermodynamics Department of CERT/ONERA) is a closed-circuit, induction-driven facility capable of runs between 30–120 s. It is pressurized, transonic, and cryogenic, and it has self-adaptive walls. Dry air is injected at ambient temperature and cooled by an injection of liquid nitrogen for cryogenic conditions.[1] The standard operating range is M_∞: 0.6–0.9, Pi_∞: 1.3–3.0 bar, and Ti_∞: 120–300 K.

The test section of the wind tunnel measures 0.39 m wide, 0.37 m high, and 1.42 m long. The flexible top and bottom walls help avoid transonic blockage and minimize wall interference effects. These walls can be controlled using either a two- or three-dimensional strategy[2,3]; they are moved by 16 hydraulic jacks acting upon invar steel sheets, allowing displacement in 0.2-mm increments up to a maximum variation

Presented as Paper 94-5.4.5 at the ICAS 19th Congress/AIAA Aircraft Systems Conference, Anaheim, CA, Sept. 18–23, 1994; received Nov. 11, 1994; revision received April 13, 1995; accepted for publication April 18, 1995.

*Research Engineer, Aerothermodynamics Department, 2 Av. Ed. Belin.
†Research Engineer, Aerothermodynamics Department, 2 Av. Ed. Belin; currently Automatics Department.
‡Head of Research Group, Aerothermodynamics Department, 2 Av. Ed. Belin.
§Research Engineer, Aerodynamics Department, 29 Av. de la Division Leclerc.

of 25 mm. The tunnel's adaptive wall capability allows relatively large models to be studied and provides very accurate results.

Besides its ability to provide high Reynolds number values, this wind tunnel is also particularly suitable for studying rear fuselage flow because its three-dimensional LDA system[4,5] allows the recording of detailed secondary fields that are crucial for measuring vortex flows.

2. Model

The 1/80th-scale model of a modern, transonic transport aircraft model was designed and manufactured at ONERA/IMF Lille. It consisted of the fuselage and a detachable horizontal rear stabilizer. The cylindrical fuselage was 0.733 m long and 0.070 m in diameter. The model differed from the real plane in having no horizontal stabilizer shield and no gap between the horizontal stabilizer and the fuselage. However, recent experiments have shown that these small modifications do not affect the main characteristics of the rear-fuselage flow, although the absence of gap would impede a possible connection between the lower and upper parts of the fuselage.

3. Experimental Setup

The model was handled in the test section using a fin-sting (Fig. 1). Because of structural problems, the model fin was geometrically different from the full-scale aircraft fin, but both the chord at the fuselage/fin junction and the sweep angle of the leading edge were correct. The sting induced interferences along the centerline of the wind tunnel, in the area where the upswept rear-fuselage would be located, but the tunnel's flexible upper and lower walls allowed this interference to be cancelled out on the fuselage axis. Velocity measurements performed during this stage of the experiment verified that the residual disturbances were small.[3]

4. Instrumentation

The model's fuselage was fitted with 139 static pressure taps, 115 of which were located on the left-hand side of the rear part, along the last 32% of its fuselage length. For two streamwise sections, taps located in the same horizontal plane helped verify that the model was not set askew. By recording so many pressure measurements in this downstream part of the fuselage it was possible to define, fairly exactly, both the streamwise evolution of pressure along the symmetry lines and the azimuthal distribution of the pressure, definitions that proved critical when examining the influence of the horizontal stabilizer on the external flow.

For wake surveys, a pressure rake was constructed. It was 125 mm wide and had two decks, the upper one consisting of eight total pressure probes and the lower one of six static ones. Apart from the two extreme total pressure probes, all of the probes were set at equal distance: 25 mm for the static probes and 15 mm for the total pressure probes. This rake was calibrated, without the model, at the beginning of the experiments but, because of its obstruction, some residual corrections were applied to the static values, using the LDA system.

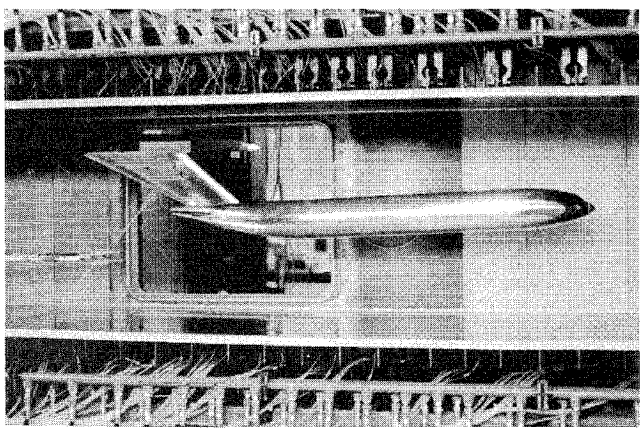

Fig. 1 View of the model in the CERT/ONERA's T2 wind tunnel, handled using a fin-sting.

The three-dimensional LDA system was used for boundary-layer and wake surveys. The diameter of the measuring volume, tightly related to the intersection of the three colored beams as well as their waists, was close to 130 μm for any configuration (forward- or backward-scattering). Regarding nearer-wall approaches, using the forward-scattering mode (tangential approach, for the symmetry lines of the model), one could go as close as 0.3–0.4 mm to the wall; however, in the backward-scattering mode (normal approach, midlateral line on the fuselage), the shortest distance to the wall was 3.0 mm.

B. Test Conditions

Tests were carried out at a stagnation pressure of 1.95 bar, at ambient temperature (300 K), for a freestream Mach number of 0.82. That led to a chord Reynolds number Re_c based on the aerodynamical chord length of the model (0.091 m), of close to 2.5×10^6.

Transition was tripped on the fuselage (carborundum band, average height: 45 μm at 12 mm from the nose) and on the lower and upper sides of the horizontal stabilizer (carborundum band, average height: 35 μm at 5% of the local chord length), but natural transition occurred on the vertical fin.

If α denotes the angle of attack of the fuselage and α_e corresponds to the setting of the horizontal stabilizer with respect to the reference horizontal fuselage line, several configurations were tested: 1) $\alpha = 0$ deg (fuselage without-stabilizer); 2) $\alpha = 2.5$ deg (fuselage without-stabilizer); 3) $\alpha = 0$ deg $- \alpha_e = -2$ deg (fuselage with-stabilizer); and 4) $\alpha = 2.5$ deg $- \alpha_e = -2$ deg (fuselage with-stabilizer).

C. Measurements

In order to reproduce the external flow around the model as accurately as possible, the adaptation of the flexible walls of the test section had to be calculated according to methods developed at DERAT.[2,3] The upper and lower flexible walls had already been adapted to the presence of the model and lateral boundary layers, but final adjustments were made for each test configuration to counteract the disturbance caused by the sting. These adjustments were made using the linearity assumption.

When the adjustments had been made, the following measurements were done: 1) oil-flow visualizations on the rear part of the fuselage and on the horizontal and vertical stabilizers; 2) streamwise pressure distributions on the rear part of the fuselage and along the upper and lower symmetry lines, azimuthal evolution of the pressure for given streamwise sections; 3) boundary-layer surveys at several streamwise abscissas along the symmetry lines of the model using the forward-scattering LDA mode; and 4) wake surveys through both velocity and pressure measurements, in one plane located at approximately two diameters downstream of the fuselage base. Pressure measurements were taken for a complete plane, but only half of the wake was measured for velocity.

These measurements were sufficient to provide a good data source for a physical understanding of the flow effects on the rear part of the fuselage.

III. Inviscid and Viscous Flow Computations

After inviscid calculations had been performed for each test configuration, boundary-layer codes were run. Then, comparisons with experimental results were investigated.

A. Potential Flow Computations

The potential flow was computed by the panel method used at ONERA, but developed at Aerospatiale.[6] This is a source-

vortex method. The surface of the aircraft is represented by quadrilateral panels, called skin panels, bearing sources of constant strength. Lifting surfaces enclose so-called skeleton panels, which support vortices of strength varying linearly in the streamwise direction, and piecewise constant in the spanwise direction. Wakes are modeled by vortices of strength equal to that of the trailing-edge skeleton panels. Flow tangency is ensured on the skin panels, and Kutta conditions are applied at the trailing edges. Compressibility is modeled according to the Prandtl–Glauert approximation.

For a half-section of fuselage there were 4320 skin panels in the fuselage with-stabilizer configuration and 3440 in the fuselage without-stabilizer configuration. Appropriate symmetry conditions completed the configurations. The grids were provided by Aerospatiale; they included the mesh of the finsting. Aerodynamic conditions were: $M_\infty = 0.82$ and α equal to 0 or 2.5 deg.

Drawings of computed isobar contours will be discussed in the following paragraphs and compared to experimental distributions.

B. Boundary-Layer Computations

The three-dimensional boundary-layer equations were solved using a characteristic method, the code for which has been rather recently developed at CERT.[7–9] The momentum equations are discretized along the local streamlines that are subcharacteristic lines; integration can maintain the same direction, independent of the crossflow direction. This method has proved valuable for applications such as prolate spheroids[8] or missiles.[9] Furthermore, one of the innovations of this method is that computations can be handled for nonregular meshes.

The system of equations (continuity, momentum, and enthalpy equations) needs boundary conditions both at the wall (impermeable wall) and at the edge of the boundary layer (data given from the solution of the inviscid flow equations). Initial laminar conditions are deduced from similarity solutions. Transition was fixed according to the experimental location on the fuselage.

Along the lower symmetry line of the rear part of the fuselage, the boundary layer grows rapidly, and its thickness is not negligible compared to the transverse curvature of the fuselage cross sections. Accordingly, a corrective term was introduced in the continuity equation, affecting mainly the derivative of the transverse component of the velocity.

The computation requires the adjunction of a turbulence model to express the components of the Reynolds shear stresses. Results presented next will include those from both a mixing length model and a two-layer model.

1) The mixing length model is the simplest model, based upon the assumption that the shear stress vector has the same direction as the velocity gradient vector. The original damping function, suggested by Van Driest and improved by Cebeci and Smith[10] to take into account streamwise pressure gradients, was considered in the relationship.

2) In the outer layer, the standard two-equation model, the original version of which was proposed by Jones and Launder,[11] was used. The transport equations for the turbulent kinetic energy k and the dissipation rate ε were solved. In the near-wall layer, only the k equation was considered, using a model originated by Bradshaw and improved later on by Wolfshein[12] and Norris and Reynolds.[13] The modeling in the outer and inner wall layers was matched at a distance to the wall corresponding to 75 wall units.

IV. Results and Discussion

In this paragraph, comparisons between experimental and computational results are presented for various aerodynamic configurations. Results for boundary-layer data will focus mainly on this configuration: $\alpha = 0$ deg, $\alpha_e = 2$ deg. On the other hand, in the wake of the model, results for both fuselage configurations will be briefly discussed.

A. Pressure Field

The concentrations of pressure taps on the rear part of the fuselage created a good picture of the pressure field in that region. Plots of the contours of constant pressure coefficient are given in Fig. 2 when the model was configured without stabilizer and with stabilizer.

Flow was almost uniform on the cylindrical part of the model. Regarding the rear part of the fuselage, the flow decelerated just ahead of the leading edge of the fin/fuselage junction. Downstream of that area, the flow then accelerated as far as the maximum cross section of the fin footprint.

There was a noticeable increase in the external velocity field in the vicinity of the flat surface, which allows rotation of the horizontal tail; that surface was restricted to 0.641 m $\leq X \leq$ 0.716 m. In either configuration of the model, these experimental data agreed closely with the computed external pressure field, although the number of pressure taps might not be enough on a given section to complete a very accurate comparison. However, important discrepancies occurred at the very end of the fuselage and near the lower symmetry line. Along that line the experimental pressure level as well as the streamwise pressure gradient differed from the computed values (Fig. 3).

In this area, the thickening of the boundary layer was significant and, consequently, the absence of coupling between

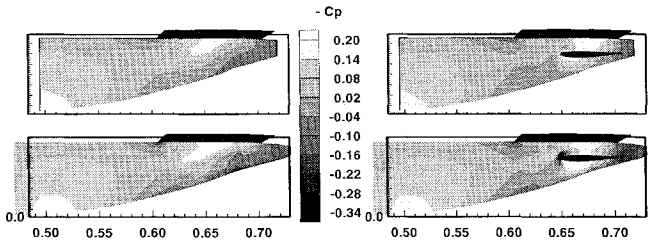

Fig. 2 Colored contours of constant pressure coefficient on the rear fuselage for $\alpha = 0$ deg – left-hand side = fuselage-without-stabilizer, right-hand side = fuselage-with-stabilizer: bottom, inviscid calculations and top, experiments.

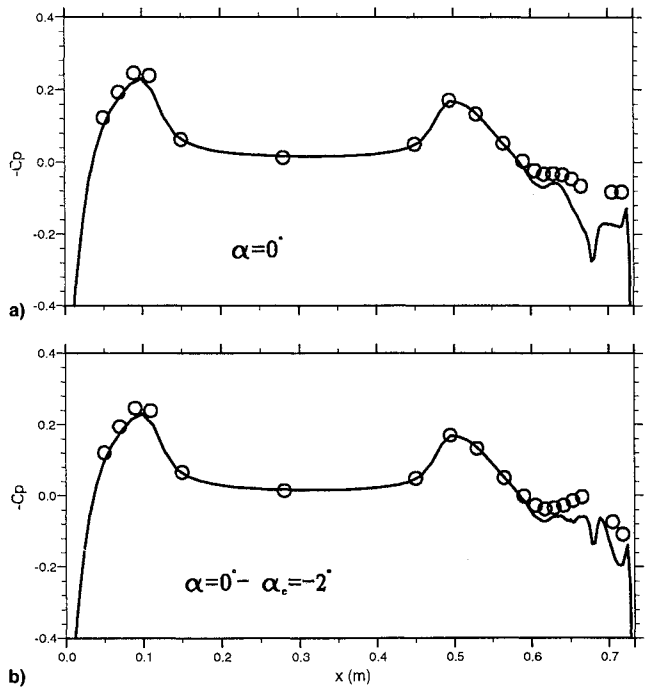

Fig. 3 Streamwise pressure gradient along the lower symmetry line. —— Inviscid calculations, ○ experiments: a) fuselage-without-stabilizer $\alpha = 0$ deg and b) fuselage-with-stabilizer $\alpha = 0$ deg – $\alpha_e = -2$ deg.

inviscid and viscous calculations could partly explain the recorded differences. The measured pressure gradient was almost equal to zero, which would suggest that the rapid growth mentioned previously balanced the decrease of the fuselage cross section.

When the horizontal stabilizer was set at -2 deg with respect to the reference horizontal fuselage line, the pressure distribution was locally altered (Fig. 2). The flow accelerated in the upper part of the fuselage, ahead of the leading edge of the horizontal tail, as well as below its lower side. These observations were more pronounced at $\alpha = 2.5$ deg than $\alpha = 0$ deg. It should be pointed out that the lift coefficient of the horizontal stabilizer was strongly negative for $\alpha = 0$ deg, but slightly positive for $\alpha = 2.5$ deg. The "negative" peak on the computed Cp distribution, around $X = 0.68$ m (Fig. 3), corresponded to a geometrical inflexion in the lower symmetry line.

B. Wall Pattern

Oil-flow visualizations were performed on different parts of the model. It is reasonable to believe that such visualizations would be a good indicator of the wall-flow pattern and allow comparisons with the computed wall streamlines or friction lines.

When the model was configured without stabilizer, visualizations showed some deviation of the wall flow downstream of the cylindrical part of the fuselage, and some weak accumulation of wall flow, concentrated along the upper and lower edges of the flat surface, which allow rotation of the horizontal tail (Fig. 4). Consequently, the vortex rollup was initiated downstream of the upsweep, its footprint clearly appearing later in the wake of the model.

Calculations revealed that tremendous wall deviations (β_0: angle between the external and friction lines) were associated with the azimuthal locations of those wall streamline accumulations; indeed, values of β_0 close to 50 deg were recorded in the lower rear part of the fuselage. The agreement with

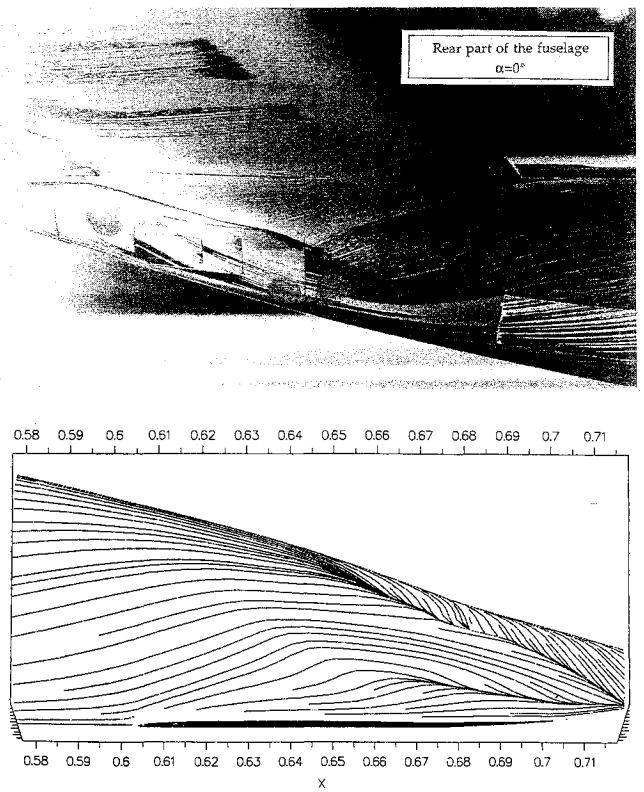

Fig. 4 Drawings of friction lines on the rear part of fuselage $\alpha = 0$ deg (fuselage-without-stabilizer), comparisons experiments/computations.

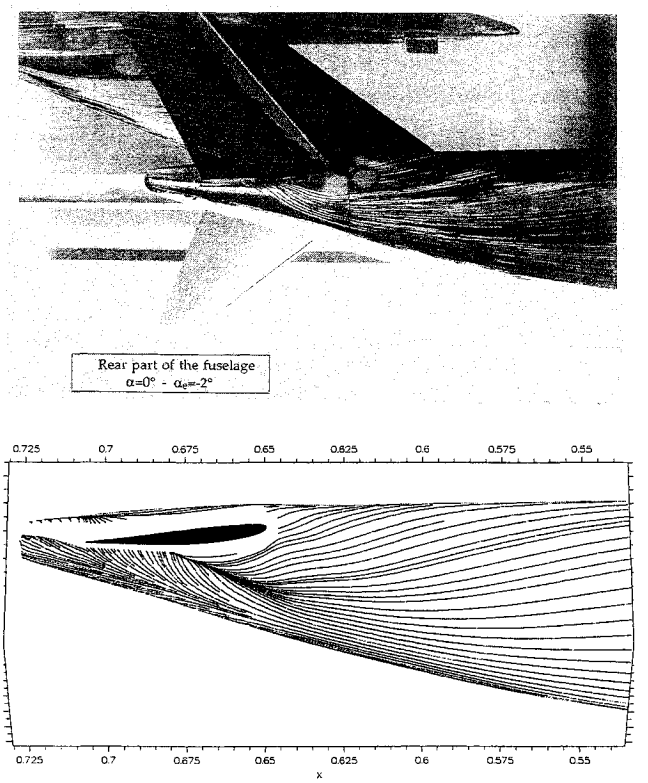

Fig. 5 Drawings of friction lines on the rear part of fuselage. $\alpha = 0$ deg $- \alpha_e = -2$ deg (fuselage-with-stabilizer), comparisons experiments/computations.

the picture resulting from the oil-flow visualization was good, but it was very hard to confirm from visualization the computed wall motion in the vicinity of the lower symmetry line. Furthermore, the computed wall-flow pattern was identical, whatever turbulence model was used.

When the fuselage configured with stabilizer, the convergence of wall streamlines was spectacular, inducing an upward motion of wall flow from the lower symmetry line towards the maximum cross section of the horizontal stabilizer (Fig. 5). The existence of intense crossflow pressure gradients, below the upstream part of the stabilizer, could induce a suction effect and, consequently, confirm such a motion. Of course, such a wall pattern gave rise to a vortex motion, the vertical development of which was restricted because of the presence of the tailplane. One could, hopefully, notice a dark triangle area on the lower side of the horizontal stabilizer, close to the junction with the fuselage, where oil could gather because of low friction.

Computations quite faithfully reproduced the recorded behaviors, although the curling motion might be weaker in the computations. Of course, in the vicinity of the tail, the boundary-layer code stopped because of the intensity of both the streamwise and azimuthal pressure gradients. It is worth mentioning that, for azimuthal locations as far as 50 deg away from the lower symmetry line, β_0 was comparable to, and even less than, the one recorded for the same value of α, but without the horizontal stabilizer.

That means that the boundary-layer development in this area is dictated by the fuselage geometry (particularly the upsweep) and not by the presence of the horizontal tail.

C. Boundary-Layer Surveys

The three-dimensional LDA measurement system allowed several boundary-layer surveys to be performed for given streamwise locations on the upper and lower symmetry lines. Velocity profiles are plotted in a coordinate system associated with the boundary layer: Y is the direction normal to the wall,

X and Z are in the plane, tangent to the wall, with X in the direction of the freestream velocity. The components of the velocity are, respectively, U, V, and W in this (X, Y, and Z) coordinate system.

For these measurements, the LDA system was operating in the forward-scattering mode in order to obtain better accuracy, measurement quickness, and access to the flow in the near-wall region. Along the lower and upper symmetry lines, the velocity component in the Z direction did not exceed 2–3 ms^{-1}, while the external freestream velocity was close to 260 ms^{-1}. This proves not only the perfect symmetry of the flow, but also that the measurement volume was correctly located along both symmetry lines.

Two surveys were performed on the upper symmetry line, in front of the fin. On the lower symmetry line, seven measurement stations were defined between $X = 0.565$–0.718 m, i.e., approximately 77 and 98% of the fuselage length.

1. Mean Quantities

For the most upstream section, the mean velocity profiles are plotted in Fig. 6, for the upper and lower symmetry lines. The considered turbulence models did not have any effect on the mean streamwise and normal to the wall velocity components. The agreement between computations and measurements was rather good, particularly on the V component, which was rather small ($|V| < 0.1U_e$).

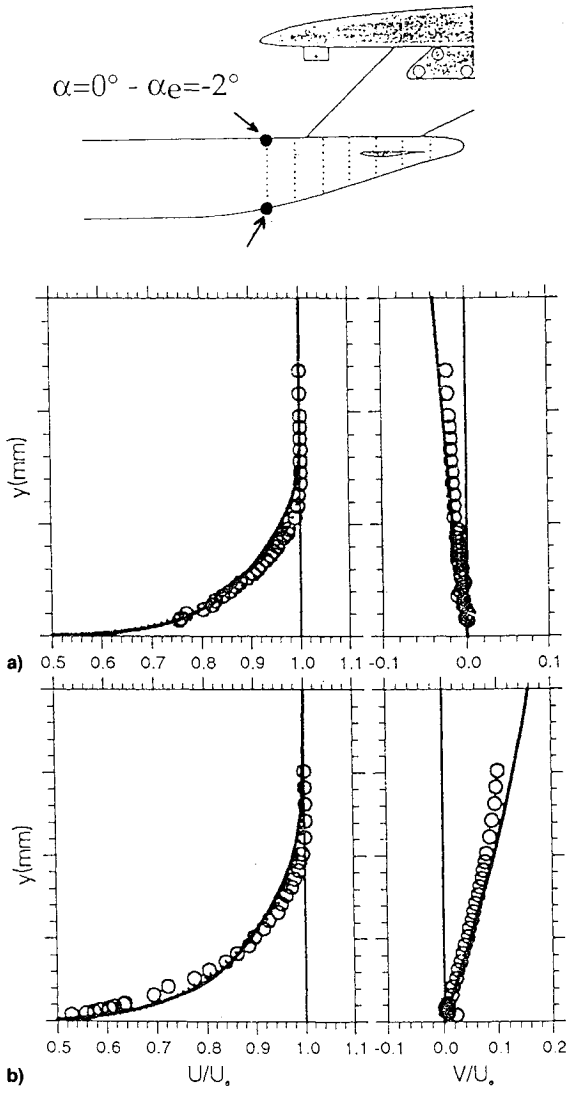

Fig. 6 Streamwise and normal to the wall velocity components at X = 0.565 m along a) upper and b) lower symmetry line. . . . Mixing length model, —— two-layer model, ○ experiments: α = 0 deg − α_e = −2 deg (fuselage-with-stabilizer).

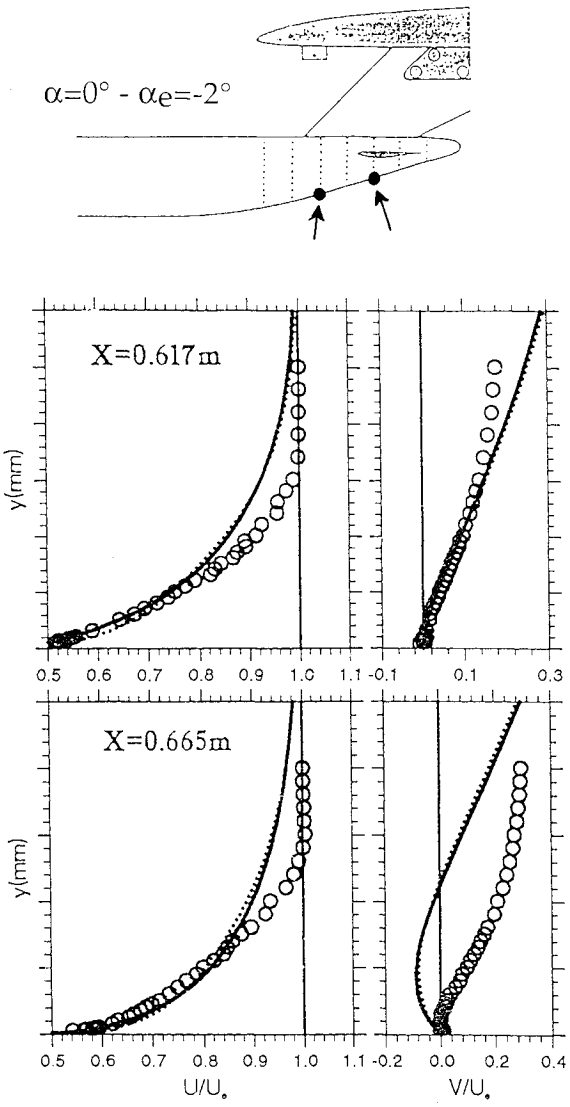

Fig. 7 Streamwise and normal to the wall velocity components along the lower symmetry line at X = 0.617 and 0.665. . . . Mixing length model, —— two-layer model, ○ experiments: α = 0 deg − α_e = −2 deg (fuselage-with-stabilizer).

Following on the development of the boundary layer along the lower symmetry line, the two components of the velocity are plotted in Fig. 7 for $X = 0.617$ and 0.665 m, respectively.

The thickening of the boundary layer was rather important at this angle of attack, approximately 15% greater than at $\alpha = 2.5$ deg. Calculation overpredicted the boundary-layer growth and, consequently, V_e appeared to be greater than the experimental value. In the outer edge of the boundary layer, the experimental value of $\partial V/\partial_x$ was equal to zero, since the pressure was roughly constant or weakly increasing. On the other hand, the computed value of $(\partial V/\partial_x)_{y=\delta}$ varied as the pressure gradient, since it is equal to $-\partial U_e/\partial_x$ (continuity equation).

Even though transverse curvature was taken into account in the continuity equation, the increase of boundary-layer thickness was large; in fact, for $X > 0.65$ m, δ was even greater than the largest dimension of the fuselage cross section. The reliability of boundary-layer assumptions in such areas is suspect. Downstream of $X = 0.617$ m, the shape of the computed U-profile was very different from the experimental one. The recorded variations on both pressure level and pressure gradient were not strong enough to explain such differences on

the two components of the mean velocity profiles. Indeed, the numerical codes that were used could not reproduce a possible interaction between the boundary-layer development along the lower symmetry line and the vortex motion that spreads downstream of the cylindric part of the fuselage.

2. Fluctuating Quantities

The shear stress and kinetic energy profiles are plotted in Fig. 8 for $X = 0.617$ and 0.665 m. Contrary to the mean velocity profiles, the turbulence model had some effect; the two-layer model provided much better results. For $X = 0.665$ m, the estimate of shear stress in the near-wall region was not satisfactory; the computed profile exhibited a rather important peak, due to the flow acceleration, while the measured shear stresses were lower. In this area where three-dimensional effects prevailed, one could question the assumption that the shear stress vector has the same direction as the mean velocity gradient vector.

The computed k profile, when applying the two-layer model, is plotted vs y, although there has been no attempt to estimate turbulent kinetic energy k, when using a mixing length model. The experimental k values were deduced from $2k = \overline{u'^2} + \overline{v'^2} + \overline{w'^2}$. Close to the wall, the turbulence level $(\sqrt{k}/U_e)$ was relatively high, and then decreased at further downstream sections; moving away from the wall, the turbulence intensity was constant over almost 30–40% of δ.

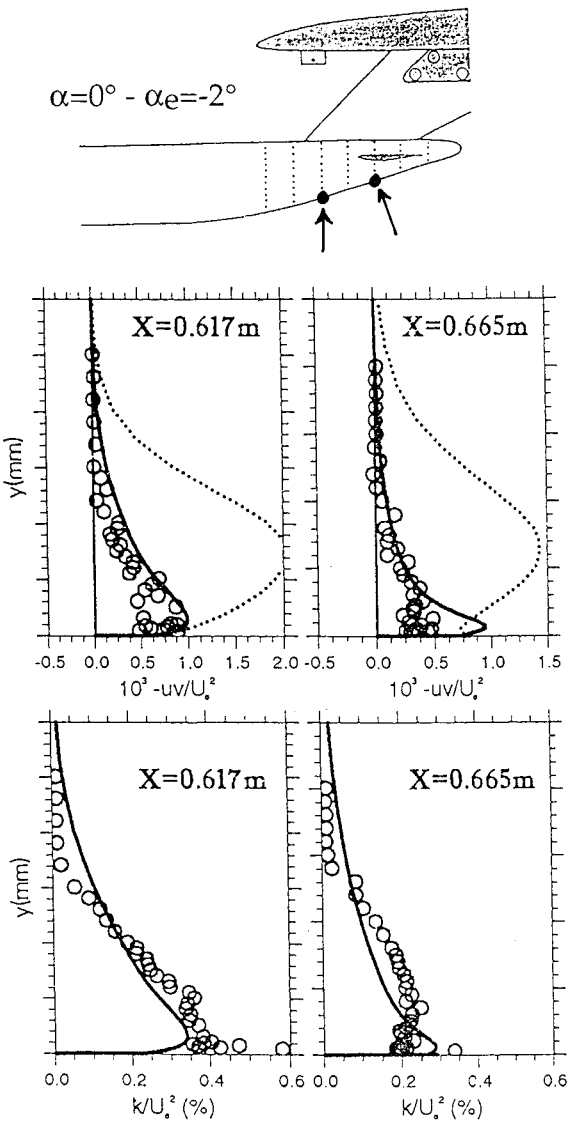

Fig. 8 Shear stress and kinetic energy profiles along the lower symmetry line at $X = 0.617$ and 0.665 m. . . . Mixing length model, —— two-layer model, ○ experiments: $\alpha = 0$ deg $- \alpha_e = -2$ deg (fuselage-with-stabilizer).

D. Wake Surveys

First of all, it is worth mentioning the good consistency of pressure and velocity measurements, from wake surveys performed in a plane located at about two diameters downstream of the fuselage base; that plane is orthogonal to the direction of the freestream. The secondary velocity field is obtained from about 600 three-dimensional LDA measurement points (forward-scattering mode), evenly distributed over a half-wake plane.

1. Pressure Measurements

The variations of the stagnation pressure in that plane are given in Fig. 9 for $\alpha = 0$ deg. The following comments can be made:

1) The symmetry of measurements was rather good, especially in the with-stabilizer configuration.

2) The wakes from the vertical and horizontal stabilizers were clearly evidenced; the maximum pressure loss downstream of the horizontal plane was roughly constant and equal to 5%.

3) For the fuselage-without-stabilizer configuration, three defect velocity pockets were recorded in the fuselage wake. The highest one came both from the fuselage base and the convergence of wall flow along the upper edge of the flat surface allowing rotation of the stabilizer; the two lowest ones, symmetrical with respect to the wake axis, seemed to be initiated from the vortex rollup, the origin of which was tightly related to the upsweep, spreading along the lower part of the fuselage. A maximum deficit of 16–17% was recorded. The shape of the wake depended upon α; its size was smaller than the maximum cross section of the fuselage.

4) In the with-stabilizer configuration, the levels of defect velocity pockets were redistributed within the wake. The effect of the tail was more pronounced at $\alpha = 0$ deg than at $\alpha = 2.5$ deg. Indeed, a sharp peak in the isobars plot could be observed; this has to be related to strong downwards negative velocities, as will be discussed later in this article.

2. Velocity Measurements

The secondary velocity field is plotted in Fig. 10 for $\alpha = 0$ deg. The gray scale of the small arrows is graduated with respect to the intensity of the local Mach number. Important vertical velocities were recorded in areas where vortex activity was intense, where Mach numbers were small, i.e., where pressure loss was greatest. Indeed, that would also suggest that pressure loss could be identified as vortex flow.

Those measurements revealed the existence of a single vortex in each half-wake plane, for the without-stabilizer config-

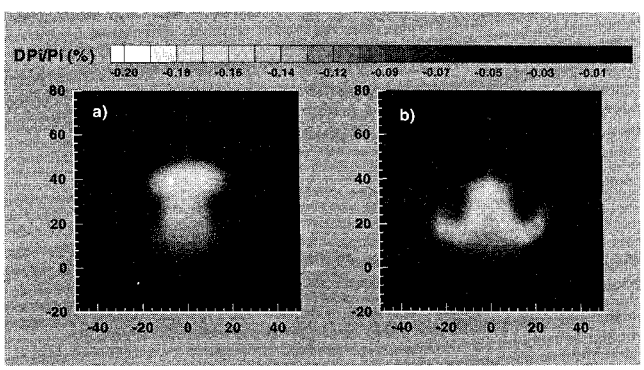

Fig. 9 Contours of constant stagnation pressure loss in the wake at two diameters downstream of the fuselage base: a) $\alpha = 0$ deg (fuselage-without-stabilizer) and b) $\alpha = 0$ deg $- \alpha_e = -2$ deg (fuselage-with-stabilizer).

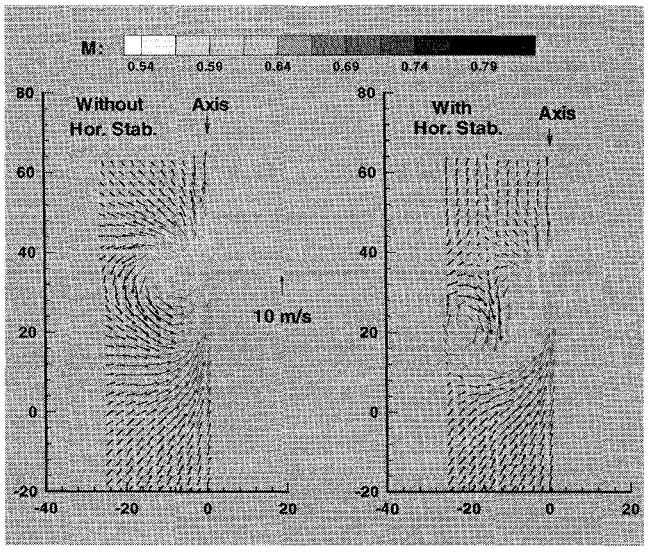

Fig. 10 Secondary velocity field at two diameters downstream of the fuselage base, for α = 0 deg; left-hand side = fuselage-without-stabilizer, right-hand side = fuselage-with-stabilizer.

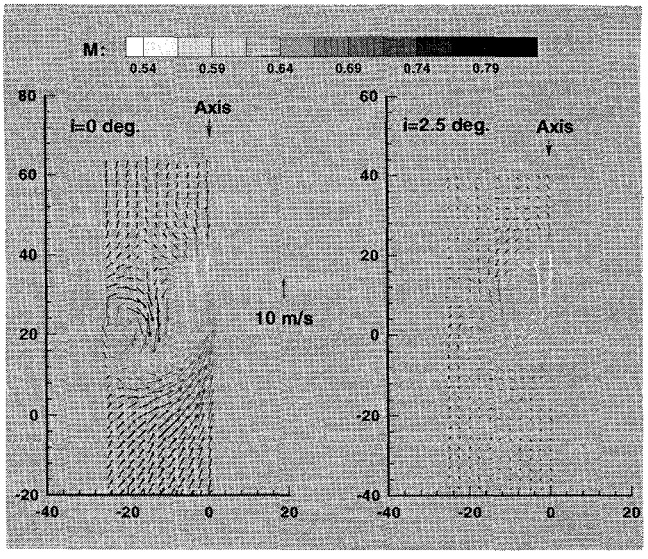

Fig. 11 Secondary velocity field at two diameters downstream of the fuselage base, for fuselage-with-stabilizer configuration; left-hand side = α = 0 deg, right-hand side = α = 2.5 deg.

uration. Its location was higher and its intensity stronger at α = 0 deg than at 2.5 deg. Along the wake centerline, rather large vertical velocities (almost 50 ms^{-1} at α = 0 deg) were recorded.

The horizontal tail generated a second contrarotating vortex in each half-plane; its center was located below the main vortex, further away from the wake axis (Fig. 11). When the fuselage was set at α = 2.5 deg, an extra "small" vortex could be identified just above the tailplane/fuselage junction.

Furthermore, at α = 0 deg, the overall fuselage wake was moving slightly downwards, according to the negative lift coefficient of the horizontal tailplane; on the other hand, this displacement effect was negligible at α = 2.5 deg. For α = 0 deg, the interaction of the two vortices created rather large negative velocity components, justifying the aforementioned sharp shape on the contours of constant stagnation pressure (Fig. 9). Knowing the two secondary velocities, it has been possible to compute the streamwise component of the rotational ($\Omega_x = \partial W/\partial Y - \partial V/\partial Z$) and, consequently, not only to define the center of each vortex system rather precisely, but also to integrate Ω_x all over each half-wake plane. By doing so, one derived an overall vorticity that was weaker for the "with-stabilizer configuration" than for the "without-stabilizer configuration," whatever the angle of attack of the fuselage.

3. Variations of Drag Coefficient

From wake surveys performed through both velocity and pressure measurements, the total drag coefficient of the model could be estimated. Indeed, pressure measurements are inadequate since they provide only the modulus of the velocity instead of the streamwise component U. On the other hand, when dealing with LDA measurements, the pressure term is omitted. Consequently, a combination of these techniques is necessary for getting a correct formulation of Cd.

Thus, by considering two planes, upstream and downstream of the model, normal to the direction of the freestream, the drag could be expressed from momentum considerations as the sum of several terms, dealing with pressure and velocity contributions:

$$Cd = Cd_{3D} + Cd_p, \qquad Cd = Cd_{2D} + Cd_{\text{vortex}} + Cd_p \tag{1}$$

where the reference surface is the total wing area at the model scale. The velocity and pressure contributions are, respectively,

$$Cd_{3D} = \frac{1}{\frac{1}{2}S_{\text{ref}}} \int_{\text{wake}} \frac{\rho U}{\rho_\infty U_\infty} \left(1 - \frac{U}{U_\infty}\right) dS \tag{2}$$

$$Cd_p = \frac{1}{\frac{1}{2}\gamma M_\infty^2 S_{\text{ref}}} \int_{\text{wake}} \left(1 - \frac{P}{P_\infty}\right) dS \tag{3}$$

Cd_{2D} is identical to Cd_{3D}, except that the streamwise velocity component is changed by the velocity modulus. By considering first-order's terms, the vortex drag component reads

$$Cd_{\text{vortex}} = \frac{1}{\frac{1}{2}S_{\text{ref}}} \int_{\text{wake}} \frac{1}{2} \frac{\rho}{\rho_\infty} \frac{(V^2 + W^2)}{U_\infty^2} dS \tag{4}$$

To estimate the drag coefficient of the fuselage alone, those equations were applied between the upstream plane (stagnation conditions) and the plane located 120 mm downstream of the model base. It was also necessary to eliminate the effects of the horizontal and vertical stabilizers. Some difficulties arose because of the strong interaction of the horizontal stabilizer and the fuselage,[14] but they were solved by following exactly the same procedure, whichever configuration was studied. This justifies the reliability of the following ΔCd values, where $\Delta Cd = Cd_{\alpha=0\text{ deg}} - Cd$.

The following results were found:

1) Increasing the angle of attack of the fuselage from α = 0 deg up to α = 2.5 deg corresponded to a decrease of the total drag coefficient of the fuselage part only: $\Delta Cd = 3.5$–4.0×10^{-4}.

2) The ΔCd induced by the presence of the horizontal stabilizer for a constant value of α was very hard to estimate, since it was almost 0.

3) The vorticity contribution in the fuselage drag balance was very dependent upon the aerodynamic configuration, but was somewhat weak.

Results could be resumed as shown in Table 1.

From the boundary-layer calculations performed for the without-stabilizer configuration, it was possible to integrate the friction vector in the surface Cartesian frame; which provided the friction drag that could be compared with the total drag, given from wake surveys.

Then, the friction drag was constant when α varied from 0 deg up to 2.5 deg, which means that the measured total drag decrease had to be allotted to the pressure drag. The contribution of friction in the drag budget was estimated to 86 and

Table 1 Drag coefficient of the fuselage part

α, deg	α_e, deg	$10^4 \Delta Cd$	Cd_{vortex}/Cd, %
0	No	—	1.84
0	−2	0.3	1.1
2.5	No	3.4	0.6
2.5	−2	4.4	0.2

90%, for $\alpha = 0$ and 2.5 deg, respectively. For the with-stabilizer configurations, computation of the total friction force was not so easy, because there were areas on the fuselage where the code stopped.

V. Conclusions

These experiments have provided a tremendous amount of data regarding the flow over the rear part of a fuselage. Tests were performed on a 1/80th-scale model of a modern, transonic transport aircraft, in CERT's transonic, pressurized T2 wind tunnel with self-adaptive walls. The model was handled within the test section by means of a fin-sting. It was set at two angles of attack, either 0 or 2.5 deg, while the horizontal stabilizer, when present, was set at −2 deg with respect to the reference horizontal fuselage line. The tests conditions consisted of a stagnation pressure close to 2 bar, ambient temperature, and a freestream Mach number of 0.82.

The combination of techniques, such as oil-flow visualizations, boundary-layer surveys and wake-flow measurements, has been a very powerful tool for understanding the physics that develops along the rear part of an upswept fuselage and in the near wake. Indeed, areas of strong crossflow associated with convergence of wall streamlines were well derived from visualizations. Boundary-layer surveys, using a three-dimensional LDA system, have pointed out the thickening of the boundary layer along the lower symmetry line of the model, whatever aerodynamic configuration was concerned. Strong stagnation pressure losses have been recorded in the wake of the model, at two diameters downstream of the fuselage base. The use of the LDA system has allowed a more precise definition of the vortex system associated with these velocity defect pockets, the intensity of the secondary velocity components in some specific areas, and the exact location of the different vortices.

The data reported in this article have helped reveal the strengths and weaknesses of inviscid and viscous codes developed or used at ONERA. For instance, results of calculations have shown a good agreement between experiments and computations for about 85% of the fuselage length, but not in the downstream part of the fuselage. It is nominally, along the lower symmetry line, where the boundary layer grows rapidly, that the comparison is far from satisfactory.

The choice of turbulence model has no influence on the mean velocity profiles, but only on the fluctuating ones. This remark is valid under the assumption that the shear stress vector has the same direction as the velocity gradient vector, which might not be true in those areas of strong three-dimensional effects.

The recorded differences between computations and experiments could be attributed to an inaccurate capture of the streamwise pressure gradient, related to a strong coupling between viscous and inviscid forces, a rather important area where three dimensionality prevails and, above all, the existence of a pressure gradient in the direction normal to the wall. The boundary-layer thickness increases rapidly and must interact with the external flow. It may be that the static pressure varies within the viscous layer. Moreover, the existence of vortex flow, generated along the rear part of the fuselage, even in the without-stabilizer configuration, would suggest that Navier–Stokes codes might apply to this rear part of the fuselage. Thus, the boundary-layer and wake data discussed in this article would be very helpful, not only for such a validation, but also for future work on turbulence modeling.

It is worth mentioning that the tests reported in this article have been followed up by further experiments in which a complete wing-body configuration has been studied, and so we are moving closer to understanding how the viscous flow around the rear fuselage is affected by both the wing and the tailplane. A good knowledge of the phenomena reported in this article could help designers optimize the shape of the rear fuselage, providing the best external and wall flows and thereby decreasing drag.

Acknowledgments

The authors gratefully acknowledge the support that Airbus Industrie and the Service Technique des Programmes Aéronautiques have provided for both the experimental and the numerical research reported in this article. Special thanks from Eric Coustols to his friend Keith Grant-Davie who very kindly improved the authors' English to the high standard required by the referees.

References

[1]Séraudie, A., Archambaud, J.-P., Blanchard, A., Dor, J.-B., and Mignosi, A., "T2 Cryogenic Transonic Wind Tunnel Thermal Design and Control of the Facility Including Models Adapted for Short Run Processing," *Proceedings of the 3rd ASME-JSME Thermal Engineering Joint Conference on Cryogenic Wind Tunnels*, Vol. 5, 1991, pp. 379–386.

[2]Archambaud, J.-P., and Mignosi, A., "The Cryogenic Adaptive Wall Wind Tunnel T2: Quality of the Adaptation with 2D and 3D Strategies, Residual Corrections, Assessment of Sidewall Effect in 2D Cases," International Conf. on Adaptive Wall Wind Tunnel Research and Wall Interference Correction, Xian, PRC, June 1991.

[3]Archambaud, J.-P., and Mignosi, A., "Techniques d'Adaptation Tridimensionnelle à la Soufflerie Transsonique T2 de l'ONERA/CERT," Internal Rept. DERAT N°49/5606.34, April 1992.

[4]Prudhomme, S., Séraudie, A., and Mignosi, A., "A Recent 3D Laser Doppler Application at the T2 Transonic Wind Tunnel: Optimisation, Experimental Results and Measurement Accuracy," 4th International Conf. on Laser Anemometry, Cleveland, OH, Aug. 1991.

[5]Mignosi, A., Séraudie, A., and Prudhomme, S., "Applications Tridimensionnelles de la Vélocimétrie Laser en Écoulement Transsonique à la Soufflerie T2," 3ème Congrès Francophone de Vélocimétrie Laser, Toulouse, France, Sept. 1992.

[6]Rivoire, V., and Eichel, P., "Méthode d'Analyse Tridimensionnelle de Systèmes Hypersustentateurs," Note Technique Aérospatiale 443.528/87, Juillet 1987.

[7]Houdeville, R., "Three-Dimensional Boundary Layer Calculation by a Characteristic Method," 5th Symposium on Numerical and Physical Aspects of Aerodynamic Flows, Long Beach, CA, Jan. 1992.

[8]Houdeville, R., Mazin, C., and Corjon, A., "Method of Characteristics for Computing Three-Dimensional Boundary Layers," *La Recherche Aérospatiale*, No. 1, 1993, pp. 37–49.

[9]Malecki, P., Cousteix, J., and Houdeville, R., "Three Dimensional Boundary Layer Calculations with Two Layer Turbulence Models," 5th International Symposium on Refined Flow Modelling and Turbulence Measurements, Paris, Sept. 1993.

[10]Cebeci, T., and Smith, A. M. O., "Analysis of Turbulent Boundary Layers," Vol. 15, *Applied Mathematics and Mechanics*, Academic, London, 1974.

[11]Jones, W. P., and Launder, B. E., "The Prediction of Laminarization with a Two-Equation Model of Turbulence," *International Journal of Heat and Mass Transfer*, Vol. 15, No. 2, 1972, pp. 301–314.

[12]Wolfshtein, M., "The Velocity and Temperature Distribution in One-Dimensional Flow with Turbulence Augmentation and Pressure Gradient," *International Journal of Heat and Mass Transfer*, Vol. 12, No. 3, 1969, pp. 301–318.

[13]Norris, L. H., and Reynolds, W. C., "Turbulent Channel Flow with a Moving Wavy Boundary," Dept. of Mech. Eng., Rept. FM-10, Stanford Univ., Stanford, CA, 1975.

[14]Séraudie, A., Mignosi, A., Dor, J. B., and Prudhomme, S., "Technique Expérimentale de Mesure en Écoulement Transsonique avec un Système de Vélocimétrie Laser Tridimensionnel. Application à la Détermination de la Traînée d'un Fuselage," AGARD 73rd FDP Meeting and Symposium on Wall Interference Support Interference and Flowfield Measurements, Brussels, Oct. 1993.